Two-domain formation during the epitaxial growth of GaN (0001) on c-planeAl2O3 (0001) by high power impulse magnetron sputtering

Junaid Muhammad, Daniel Lundin, Justinas Palisaitis, Ching-Lien Hsiao,
Vanya Darakchieva, Jens Jensen, Per Persson, Per Sandström, W-J Lai, L-C Chen, K-H Chen,
Ulf Helmersson, Lars Hultman and Jens Birch

Linköping University Post Print

N.B.: When citing this work, cite the original article.

Original Publication:

Junaid Muhammad, Daniel Lundin, Justinas Palisaitis, Ching-Lien Hsiao, Vanya Darakchieva, Jens Jensen, Per Persson, Per Sandström, W-J Lai, L-C Chen, K-H Chen, Ulf Helmersson, Lars Hultman and Jens Birch, Two-domain formation during the epitaxial growth of GaN (0001) on c-planeAl2O3 (0001) by high power impulse magnetron sputtering, 2011, Journal of Applied Physics, (110), 123519.
http://dx.doi.org/10.1063/1.3671560
Copyright: American Institute of Physics

Postprint available at: Linköping University Electronic Press
http://urn.kb.se/resolve?urn=urn:nbn:se:liu:diva-73296

AIP | Journal of Applied Physics

Two-domain formation during the epitaxial growth of GaN (0001) on c-plane Al2O3 (0001) by high power impulse magnetron sputtering

M. Junaid, D. Lundin, J. Palisaitis, C.-L. Hsiao, V. Darakchieva et al.

Citation: J. Appl. Phys. **110**, 123519 (2011); doi: 10.1063/1.3671560

View online: http://dx.doi.org/10.1063/1.3671560

View Table of Contents: http://jap.aip.org/resource/1/JAPIAU/v110/i12

Published by the American Institute of Physics.

Related Articles

Local structural models of complex oxygen- and hydroxyl-rich GaP/InP(001) surfaces
J. Chem. Phys. 136, 064705 (2012)

Well-arranged novel InGaN hexagonal nanoplates at the tops of nitrogen-polarity GaN nanocolumn arrays
AIP Advances 2, 012140 (2012)

Single photon emission from InGaN/GaN quantum dots up to 50K
Appl. Phys. Lett. 100, 061115 (2012)

Near-infrared nano-spectroscopy of semiconductor quantum dots using a phase-change mask layer
Appl. Phys. Lett. 100, 063111 (2012)

Position-controlled [100] InP nanowire arrays
Appl. Phys. Lett. 100, 053107 (2012)

Additional information on J. Appl. Phys.

Journal Homepage: http://jap.aip.org/

Journal Information: http://jap.aip.org/about/about_the_journal

Top downloads: http://jap.aip.org/features/most_downloaded

Information for Authors: http://jap.aip.org/authors

ADVERTISEMENT

Downloaded 13 Feb 2012 to 130.236.83.30. Redistribution subject to AIP license or copyright; see http://jap.aip.org/about/rights_and_permissions

Two-domain formation during the epitaxial growth of GaN (0001) on *c*-plane Al_2O_3 (0001) by high power impulse magnetron sputtering

M. Junaid,[1,a)] D. Lundin,[1] J. Palisaitis,[1] C.-L. Hsiao,[1] V. Darakchieva,[1] J. Jensen,[1] P. O. Å. Persson,[1] P. Sandström,[1] W.-J. Lai,[2] L.-C. Chen,[2] K.-H. Chen,[2,3] U. Helmersson,[1] L. Hultman,[1] and J. Birch[1]
[1]*Department of Physics, Chemistry and Biology (IFM), Linköping University, SE-581 83 Linköping, Sweden*
[2]*Center for Condensed Matter Sciences, National Taiwan University, Taipei 106, Taiwan*
[3]*Institute of Atomic and Molecular Sciences, Academia Sinica, Taipei, Taiwan*

(Received 19 July 2011; accepted 20 November 2011; published online 23 December 2011)

We study the effect of high power pulses in reactive magnetron sputter epitaxy on the structural properties of GaN (0001) thin films grown directly on Al_2O_3 (0001) substrates. The epilayers are grown by sputtering from a liquid Ga target, using a high power impulse magnetron sputtering power supply in a mixed N_2/Ar discharge. X-ray diffraction, micro-Raman, micro-photoluminescence, and transmission electron microscopy investigations show the formation of two distinct types of domains. One almost fully relaxed domain exhibits superior structural and optical properties as evidenced by rocking curves with a full width at half maximum of 885 arc sec and a low temperature band edge luminescence at 3.47 eV with the full width at half maximum of 10 meV. The other domain exhibits a 14 times higher isotropic strain component, which is due to the higher densities of the point and extended defects, resulting from the ion bombardment during growth. Voids form at the domain boundaries. Mechanisms for the formation of differently strained domains, along with voids during the epitaxial growth of GaN are discussed. © *2011 American Institute of Physics.* [doi:10.1063/1.3671560]

I. INTRODUCTION

Group III-nitrides such as InN, GaN, and AlN combine direct bandgaps ranging from 0.65 to 6.1 eV with a high breakdown voltage and high electron mobility.[1–3] They attract much attention due to their opto-electronic properties. Bandgap engineering of their ternary alloys allows for the tuning of their physical properties for applications such as light emitting diodes (LEDs) and laser diodes covering the spectral wavelength from infrared to ultraviolet.[4–6] Solid-state lighting devices based on group III-nitride materials, including LEDs, are thus foreseen to replace incandescent light bulbs and florescent lamps with a substantial impact on energy savings.[7]

We investigate GaN, which has a direct bandgap of 3.4 eV.[2] For example, for opto-electronic applications at room temperature, the GaN must be of high purity and high crystalline quality with a low defect density. Chemical vapor deposition (CVD) and molecular beam epitaxy (MBE) are the most common techniques used to grow GaN today. During the growth by CVD high temperatures ranging from 900 to 1050 °C are used, which puts limitations on the choice of substrate. In the case of MBE it is possible to grow at lower temperatures such as 700 °C, however, the method has high running costs and is limited to small substrates.[1,8]

Magnetron sputter epitaxy (MSE) offers an alternative route to the III-N epitaxial layers.[9] Magnetron sputter epitaxy employs low-energy (20–30 eV) ion bombardment to enhance adatom mobility at low substrate temperatures. Scalability and technological maturity in industrial applications are the major advantages in using sputtering. However, for the reactive sputter deposition of electronic-grade GaN, there are difficulties in obtaining stable growth conditions. These are mainly caused by the low melting point (29 °C) of the metallic Ga target and the formation of a non-conducting GaN layer on its surface. On the contrary, mastering reactive sputtering from a liquid target can give clear process advantages such as a high deposition rate, the elimination of target erosion effects, and the possibility of a continuous supply of the source material.

High power impulse magnetron sputtering (HiPIMS) generates a process plasma with energetic metal ions that is 2-3 orders of magnitude more dense than for direct current magnetron sputtering (DCMS).[10,11] The energetic species in such plasmas may be utilized to stimulate epitaxal growth at low temperatures.[12] In addition, it has been shown that HiPIMS may lead to a substantial reduction of the hysteresis effect present in reactive magnetron deposition processes. In a reactive sputtering process the reactive gas (in our case, it is N_2) reacts with the target material (Ga) and may form a thin layer of a compound (GaN) on the target surface. This phenomenon, known as target poisoning, has a negative effect on the sputtering rate. However, in the case of HiPIMS, this effect is reduced as compared to DCMS,[13] which yields a high deposition rate and more stable operating conditions.

In this work we explore the effects of applying high power pulses in the MSE of GaN for the growth of μm-thick epitaxial films that contain domains of different strain levels. X-ray diffraction (XRD), reciprocal space mapping (RSM), and micro-Raman (μ-Raman) characterization techniques were used to identify the types and amount of strain in these

[a)]Electronic mail: junmu@ifm.liu.se.

 © 2011 American Institute of Physics

Downloaded 13 Feb 2012 to 130.236.83.30. Redistribution subject to AIP license or copyright; see http://jap.aip.org/about/rights_and_permissions

domains. The surface morphology was studied by atomic force microscopy (AFM). The structural properties and the micro-structural evolution of the grown films were investigated by using cross-sectional transmission electron microscopy (XTEM) and scanning transmission electron microscopy (STEM). The optical properties of different domains were studied by room and low temperature micro-photoluminescence (μ-PL). Room temperature cathodoluminescence (CL) imaging was also used to see the spatial distribution of optically active domains at room temperature. Furthermore, we discuss different reasons for the formation of different domains and also suggest solutions to optimize the growth of GaN.

II. EXPERIMENTAL DETAILS

The GaN was epitaxially grown on (0001)-oriented Al_2O_3 substrates without any buffer layer by HiPIMS. The growth was performed in a UHV chamber having a base pressure of $<10^{-8}$ Torr. Liquid Ga (99.99999% pure), contained in a horizontal water cooled stainless steel trough 50 mm in diameter, was used as a sputtering target. To form GaN, a mixture of Ar (99.999999% pure) and N_2 (99.999999% pure) was used at a constant total pressure of 16 mTorr. A custom built HiPIMS power supply was used during these experiments. Pulses up to approximately 680 V and 1.5 A were used with a pulse duration of 30 μs and a repetition frequency of 800 Hz. These discharge conditions resulted in an average power of 14 W to the sputtering target. A typical HiPIMS pulse shape is shown in Fig. 1. The substrate temperature was 700 °C. In order to ensure a stable temperature, indirect heating from the back side of the substrate was used and controlled by a thermocouple, calibrated by infrared pyrometry.

An initial series of ~190 nm thick GaN (0001) films were grown at different N_2 partial pressures (P_{N2}), ranging from 4 to 12 mTorr, with the purpose of optimizing the pressure window with respect to the GaN crystallinity and stoichiometry. In a second series, ~1100 nm thick films were grown at an optimized P_{N2} ranging from 8 to 10 mTorr.

The elemental composition of the as-deposited films was obtained by time-of-flight elastic recoil detection analysis (ToF ERDA). Here, 40 MeV $^{127}I^{9+}$ ions were used as projectiles along with a recoil angle of 45° with the incident angle set to 22.5° relative to the surface. The measured recoil ToF ERDA spectra were converted into relative atomic concentration profiles using the CONTES code.[14,15]

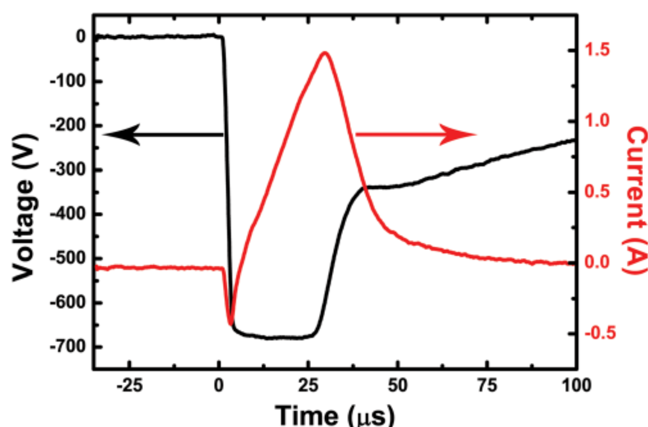

FIG. 1. (Color online) Voltage and current evolution during a typical HiPIMS pulse used during the growth experiments.

To study the morphology of the grown films, a Dimension 3100 atomic force microscope (AFM) was used in tapping mode.

Overview θ-2θ x-ray diffraction scans were performed with a Philips 1820 Bragg-Brentano diffractometer. For high-resolution x-ray diffraction (HRXRD) measurements, a Philips X'Pert MRD diffractometer was used, equipped with a graded parabolic x-ray mirror and a channel-cut Ge (220) single-crystal monochromator which produces a highly collimated beam of pure Cu $K\alpha_1$-radiations ($\lambda = 0.15406$ nm). The diffracted beam was analyzed using an asymmetric double-bounce Ge (220) crystal collimator. High resolution reciprocal space mapping (RSM) was carried out in symmetric and asymmetric scattering geometries using the GaN 0002 and $10\bar{1}5$ reflections, respectively.

The microstructure of the as-deposited GaN films was investigated by XTEM and also by STEM using a FEI Tecnai G2 TF 20 UT field-emission TEM operated at 200 kV. For the dark field STEM imaging, a high angle annular dark field imaging (HAADF-STEM) mode was used. Two different samples were prepared for TEM analysis. The XTEM sample was prepared by mechanical polishing followed by Ar ion milling at 5 keV. The final polishing was done using low energy ions at 2 keV. In order to selectively make a cross-sectional sample of individual features in the epilayers, a cross sectional sample was prepared by using a Carl Zeiss Crossbeam 1540 EsB focused ion beam milling instrument and this sample was used for the STEM analysis.

To characterize the spatial distribution of the strained material, μ-Raman mapping and spectroscopy (Jobin-Yvon T64000, 0.35 cm^{-1} resolution) were performed on the GaN samples in backscattering geometry at room temperature. The experimental details can be found in Refs. 16 and 17.

The optical properties at room and low temperature (i.e., at 4 K) were characterized by μ-PL in a backscattering geometry. A continuous-wave Coherent Verdi/MBD-266 laser system ($\lambda_{exc} = 266$ nm) was used as an excitation source with the laser beam focused down to ~2 μm in diameter by a 50 × refractive objective. The collected PL light was dispersed by a single-grating monochromator with a spectral resolution better than 0.2 nm in the 300–600 nm range and detected by a liquid-nitrogen-cooled charge coupled device.

Cathodoluminescence (CL) studies were also performed by using a LEO field emission scanning electron microscope equipped with an Oxford Research Instrument CL spectrometer. The experimental details can be found in Ref. 18.

III. RESULTS AND DISCUSSION

In order to find an optimized process window in terms of N_2 partial pressure, HRXRD $2\theta/\omega$ scans and ω scans were performed for the initial series of 190 nm thick GaN films grown at N_2 partial pressures (P_{N2}) ranging from 4 to 12 mTorr. Figure 2 shows the full width at half maximum

Downloaded 13 Feb 2012 to 130.236.83.30. Redistribution subject to AIP license or copyright; see http://jap.aip.org/about/rights_and_permissions

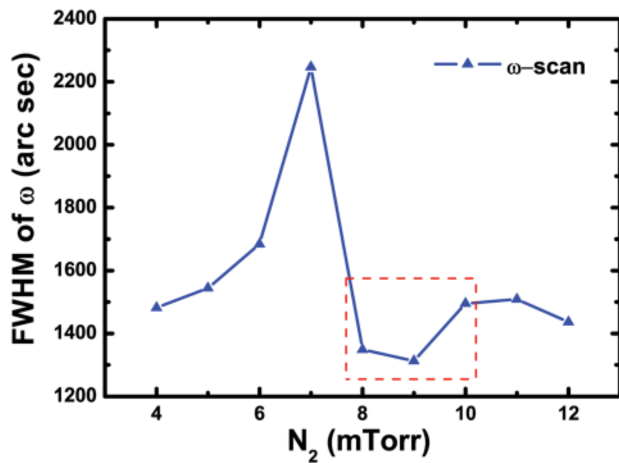

FIG. 2. (Color online) FWHM of ω (0002) HRXRD scans vs the N_2 partial pressure of the ~190 nm thick GaN epilayers. The rectangle indicates the pressure window for which the thicker samples were grown.

(FWHM) of the ω scan for the GaN 0002 peak for all the samples in the first series. It can be seen that a minimum is obtained in ω-FWHM for P_{N2} between 8 and 10 mTorr, exhibiting an optimum in crystal quality, i.e., a minimum in screw type dislocations (mosaic tilt) and a maximum in the lateral coherence length.[19] The ω-FWHM minimum coincides with a minimum in the $2\theta/\omega$-FWHM (not shown) indicating larger diffracting regions in the layer for that pressure range as well. Figure 3(a) shows a $2\theta/\omega$ Bragg-Brentano scan of the sample grown at $P_{N2} = 9$ mTorr, covering a wide range, which only exhibits the GaN 0002 and Al_2O_3 0006 peaks. Figure 3(b) shows the HRXRD $2\theta/\omega$ scan of the 0002 GaN peak located at ~34.468°, which corresponds to biaxially compressed GaN. The FWHM of the $2\theta/\omega$ peak is 291 arc sec, indicating that the x-rays are coherently scattered by regions extending more than 100 nm in the growth direction.

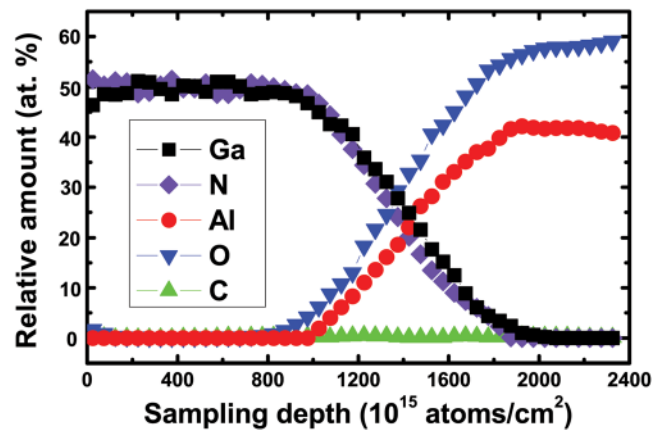

FIG. 4. (Color online) ToF-ERDA elemental depth profile of a ~190 nm thick GaN film.

The larger FWHM, as observed outside the optimum P_{N2} range, means smaller vertical coherence lengths, implying less perfect crystallinity and/or smaller domains. The ω-FWHM around the GaN 0002 peak is 1300 arc sec.

An ERDA compositional depth profile, obtained from a ~190 nm thick GaN epilayer and grown at $P_{N2} = 9$ mTorr, is shown in Fig. 4. The results are similar to those obtained at $P_{N2} = 8$ and 10 mTorr and show that all the films in that P_{N2} range are stoichiometric. The Ga and N concentrations are close to stoichiometry, 49.8 ± 0.5 and 49.9 ± 0.5 at. %, respectively. The O content is 0.2 at. %, just above the detection limit, and the C content is too close to its detection limit of 0.1 at. % to be significant. The origin of the increased C-signal at the surface and the interface is unknown, however, it may stem from physisorbed hydrocarbons at the surface prior to and after growth. Possible sources of O are post growth surface oxidation and in-diffusion along threading defects.

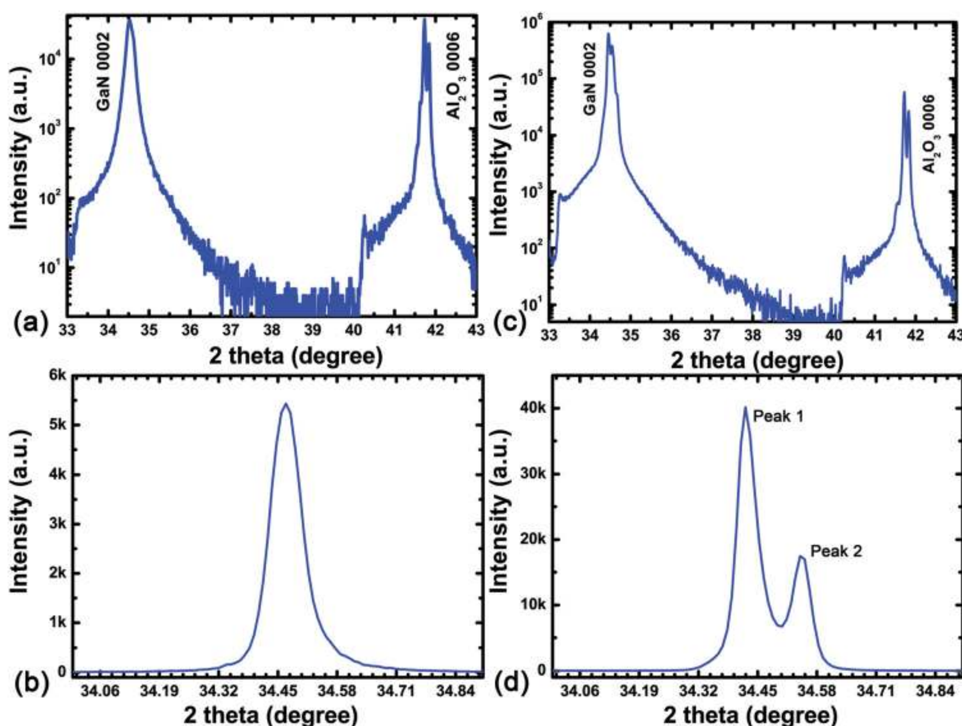

FIG. 3. (Color online) (a) The XRD (Bragg-Brentano) scan of a thin sample grown at $P_{N2} = 9$ mTorr, showing a GaN 0002 peak and the substrate peak, and (b) the HRXRD $2\theta/\omega$ short range scan around the GaN 0002 peak position. (c) The XRD (Bragg-Brentano) scan of a ~1100 nm thick sample grown at $P_{N2} = 9$ mTorr, showing the GaN 0002 peak and the substrate peak, and (d) the HRXRD $2\theta/\omega$ short range scan around the GaN 0002, showing a splitting of the peak indicating the existence of strained (Peak 1) and almost relaxed (Peak 2) domains.

Downloaded 13 Feb 2012 to 130.236.83.30. Redistribution subject to AIP license or copyright; see http://jap.aip.org/about/rights_and_permissions

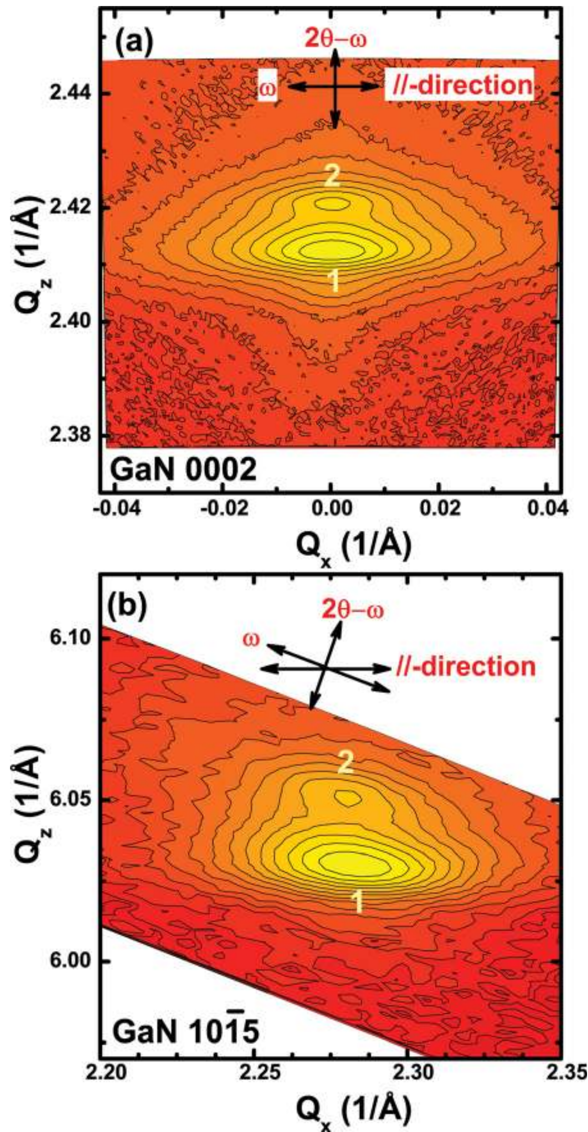

FIG. 5. (Color online) Symmetric and asymmetric reciprocal space maps around the 0002 and 10$\bar{1}$5 reflection from the ~1100 nm thick sample grown at $P_{N2} = 9$ mTorr. The diffraction from the more strained GaN is indicated by "1" while "2" indicates the diffraction from the less strained GaN.

Based upon the preceding results, we conclude that it is possible to grow high-quality (pure, stoichiometric, and single-crystal) 0002 oriented GaN films using HiPIMS. Further material characterization was focused on thicker epilayers grown using the optimal N_2 partial pressures of 8, 9, and 10 mTorr. The results from these samples did not differ significantly from each other. Therefore, we choose to report data from the 9 mTorr sample in this article.

Figure 3(c) shows a long range XRD (Bragg-Brentano) scan of the ~1100 nm thick sample grown at $P_{N2} = 9$ mTorr. In the graph, only a single GaN 0002 peak at ~34.468° along with the substrate 0006 peak can be seen. In the HRXRD $2\theta/\omega$ scan shown in Fig. 3(d), the GaN 0002 peak is seen to consist of two closely spaced peaks indicating the presence of two domains with different *c* lattice parameters. Since ERDA showed stoichiometric films, this difference is likely due to the presence of varying strain levels within different areas of the film. The position of the more intense peak 1, at $2\theta = 34.4207°$, indicates an expansion of the lattice along the c-axis. The weaker peak 2, at $2\theta = 34.5461°$, is very close to the position for relaxed bulk GaN, i.e., $2\theta = 34.5794°$,[2] indicating that it emanates from less strained domains of the sample. The domains in the sample corresponding to peaks 1 and 2 will, from now on, for simplicity, be denoted as "more strained" and "less strained," respectively.

The ω-FWHM values of peak 1 and peak 2 are ~1040 and ~885 arc sec, respectively. The values of the FWHMs of both more strained and less strained domains indicate a high structural order, where the less strained domains have a better structural quality than the more strained domains. In order to determine the *a* and *c* lattice parameters, RSMs were recorded around the 0002 and 10$\bar{1}$5 peaks. Figure 5(a) shows the symmetric RSM around the 0002 reflection and Fig. 5(b) represents the asymmetric RSM around the 10$\bar{1}$5 reflection of the thicker film grown at $P_{N2} = 9$ mTorr. Two different peaks are clearly detected in RSM; one corresponding to the more strained part (1) and the other to the less strained part (2) of the epilayer. The respective *a* and *c* lattice parameters for both domains, obtained from the RSMs shown in Fig. 5, are listed in Table I. Additionally, the total strains along the *a* (ε_a) and *c* (ε_c) directions are calculated by using Eq. (1) and are shown Table I,

$$\varepsilon_c = \frac{c - c_o}{c_o}, \quad \varepsilon_a = \frac{a - a_o}{a_o}, \tag{1}$$

where $a_o = 3.18926$Å and $c_o = 5.18523$Å (Ref. 20) are the reference lattice parameters for relaxed bulk GaN. Both the more strained and the less strained domains experience in-plane compression and expansion along the c-axis, which is normally attributed to the presence of pure biaxial strain, caused by the difference in the lattice parameters and thermal expansion coefficients of GaN and sapphire. Under biaxial strain, the surface is free to expand or contract and therefore the in-plane, ε_a, and the out-of-plane, ε_c, strain components are related via Eq. (2),[21]

$$\frac{\varepsilon_c}{\varepsilon_a} = -\frac{2C_{13}}{C_{33}} \approx -0.598, \tag{2}$$

TABLE I. Measured values of the *a* and *c* parameters and total strain along the in-plane and the out-of-plane directions are shown. The calculated isotropic strain component for both more and less strained domains are also shown.

N_2 partial pressure and domain type	*a* (Å)	*c*(Å)	In-plane strain, ε_a	Out-of-plane strain, ε_c	Isotropic strain, ε_{iso}
9 mTorr, more strained	3.1778	5.2098	−0.00359	0.00474	0.00162
9 mTorr, less strained	3.1814	5.1919	−0.00246	0.00129	−0.00011

Downloaded 13 Feb 2012 to 130.236.83.30. Redistribution subject to AIP license or copyright; see http://jap.aip.org/about/rights_and_permissions

where C_{13} and C_{33} are stiffness constants. We use the values for the stiffness constants: $C_{11} = 365$ GPa, $C_{12} = 135$ GPa, $C_{13} = 114$ GPa, and $C_{33} = 381$ GPa, as reported in Ref. 22. The ratio, $\varepsilon_c/\varepsilon_a$, estimated using the experimental total strain values (from Table I) is -1.32 for the more strained domains and -0.524 for the less strained domains. The latter is very close to the expected value estimated by Eq. (2), confirming a predominantly biaxial strain in the less strained domains. On the contrary, for the more strained domain, the ratio between the out-of-plane and in-plane strain components is significantly larger than -0.598 in magnitude. This behavior could be explained by a coexistence of biaxial and isotropic strain components in the film, as has previously been reported for high quality GaN films grown by DC-MSE on Al_2O_3 substrates.[9] In such a case, the measured total strain can be treated as the sum of the pure biaxial strain components, $^*\varepsilon_a$ and $^*\varepsilon_c$, and the isotropic strain component, ε_{iso},[23]

$$\begin{aligned} \varepsilon_c &= \varepsilon_c^* + \varepsilon_{iso}, \\ \varepsilon_a &= \varepsilon_a^* + \varepsilon_{iso}. \end{aligned} \tag{3}$$

The isotropic stain component, ε_{iso}, was deconvoluted using Eqs. (2) and (3) and can be represented by Eq. (4),

$$\varepsilon_{iso} = \frac{2C_{13}\varepsilon_a + C_{33}\varepsilon_c}{2C_{13} + C_{33}}. \tag{4}$$

From Table I, it is clear that some isotropic strain is present in both the more strained and the less strained domains, however, the isotropic strain component in the more strained domain is almost 14 times higher. The origin of such a high isotropic strain component in the GaN can be point defects, induced by plasma-surface interactions, causing an isotropic lattice expansion. In addition, the O impurities present in the films (see Fig. 4) can also contribute to such an isotropic expansion of the GaN lattice.[24] Thus, these results suggest a higher point defect density in the more strained domains compared to the less strained domains, where the isotropic strain component is negligible. Comparing these results with the GaN epilayers grown by direct current-magnetron sputter epitaxy (DC-MSE), reported by Junaid *et al.*,[9] the isotropic strain component in the more strained domains is nearly 4 times higher when using HiPIMS, while the less strained domains exhibit a nearly 4 times lower isotropic strain component than the DC-MSE case. Thus, if the formation of the more relaxed domains can be controlled and promoted, HiPIMS may have the potential of high quality GaN epilayer growth.

The surface morphologies of the samples grown at $P_{N2} = 9$ mTorr using AFM are shown in Fig. 6. The thin sample exhibits circular surface features (disks) with an average diameter of ~1 μm, and an average height of ~20 nm (see Fig. 6(a)). The surface morphology of the thick sample grown at $P_{N2} = 9$ mTorr is shown in Fig. 6(b). The corresponding surface features have an average diameter of ~3-4 μm and a height of ~200 nm, however, the density of features is not significantly different from the thin samples. We thus conclude that the large features appearing on the surface of the thick samples nucleate in the early stages of the growth, whereafter they grow in height at a higher rate than the film growth rate.

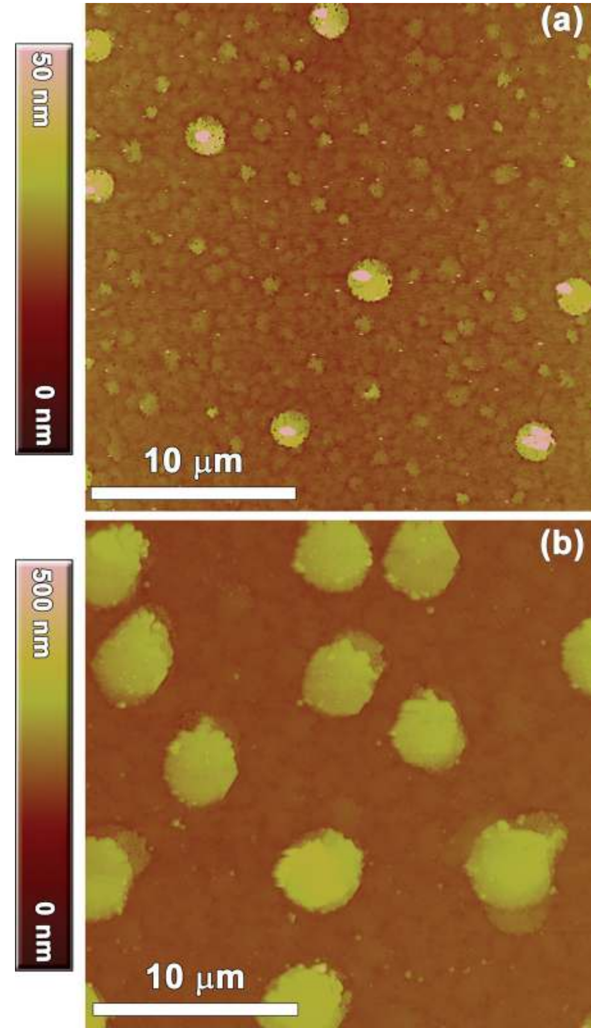

FIG. 6. (Color online) AFM images. (a) Surface morphology of a ~190 nm thick GaN layer grown at $P_{N2} = 9$ mTorr. The surface features have a diameter of ~1 μm, a height of ~20 nm, and the surface RMS roughness value is ~6 nm. (b) Surface morphology of a ~1100 nm thick GaN layer grown at $P_{N2} = 9$ mTorr. The surface features have a diameter of ~3–4 μm, a height of ~200 nm, and the surface RMS roughness of ~36 nm.

The AFM results support our HRXRD results showing that there are two different types of domains. In order to identify which part is less strained and which is more strained, we performed μ-Raman spectroscopy and mapping measurements on the samples. Figure 7(a) shows the μ-Raman spectra from two different regions of the GaN film grown at $P_{N2} = 9$ mTorr. The spectra revealed the allowed E_2 (high) vibrational mode. The less intense spectrum, which was recorded from a flat area in between the features as observed by AFM, is peaked at 571 cm^{-1}. It is blue shifted with respect to the strain-free E_2 wave number of 567.6 cm^{-1} (Refs. 25 and 26) and indicates the presence of compressive biaxial strain in the film. The more intense spectrum that was taken from one of the circular features (see the AFM image in Fig. 6(b)) has the E_2 mode peaked at 569.9 cm^{-1}, which is closer to the bulk GaN value. This shows that the features predominantly consist of the "less

Downloaded 13 Feb 2012 to 130.236.83.30. Redistribution subject to AIP license or copyright; see http://jap.aip.org/about/rights_and_permissions

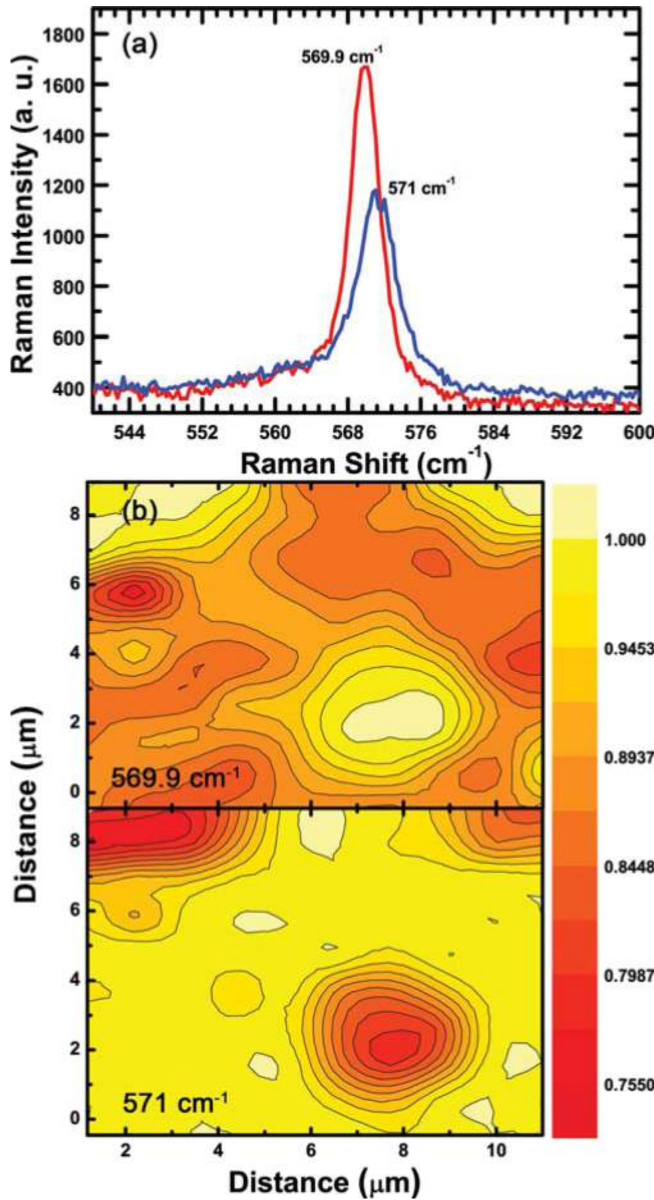

FIG. 7. (Color online) (a) The μ-Raman spectra from two different domains having different strain levels. (b) Two μ-Raman maps over the same area using the wave numbers (frequencies) in Fig. 7(a), confirming the presence of domains with different strains in the sample.

strained" GaN and that the areas in between can be identified as the "more strained" regions. This spatial distribution of the less and more strained domains is clearly demonstrated by the two μ-Raman maps for the 569.9 and 571 cm^{-1} wave numbers, as shown in Fig. 7(b), which shows complementary intensity distributions. The 569.9 cm^{-1} map exhibits a strong peak at the feature with low intensity from its surroundings, while the 571 cm^{-1} map exhibits a corresponding clear minimum at the feature, and an even intensity from the area in between the features. The narrower FWHM $\sim$4 cm^{-1} and higher Raman intensity detected from the relaxed domains indicate a better structural order, which is in agreement with the HRXRD results. The shift in frequency, $\Delta\omega_\lambda$, of the E_2 (high) vibrational mode is related to the in-plane ε_a strain components in the film via,[27]

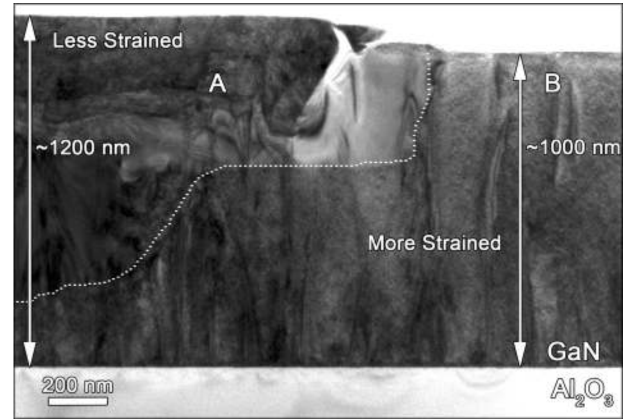

FIG. 8. XTEM micrograph of a thick sample grown at $P_{N2} = 9$ mTorr, clearly showing two different domains. The boundary between the less strained (A) and the more strained (B) domains is marked by the dashed line.

$$\Delta\omega_\lambda = \left(2a_\lambda - \frac{2C_{13}}{C_{33}} b_\lambda\right)\varepsilon_a, \tag{5}$$

where $a_\lambda = -742$ cm^{-1} and $b_\lambda = -727$ cm^{-1} are the E_2 deformation potentials, as obtained from Ref. 21. Using Eq. (5), we have estimated an in-plane strain in the less strained domain of -0.00219 and for the more strained domain we obtained a value of -0.00324. These results are in good agreement with the XRD biaxial strain components (see Table I). The set of stiffness constants and deformation potentials used was found to affect the values of the strain within 10%. The best agreement between the strain values measured by XRD and estimated from the Raman shift is obtained for the stiffness constants reported in Ref. 22 and using the deformation potentials reported in Ref. 21.

To gain further insight into the structural properties and evolution during growth, XTEM was performed. Figure 8 shows an XTEM micrograph of a thick sample grown at $P_{N2} = 9$ mTorr. From the difference in contrast and the surface morphology, one can clearly locate the two types of domains. The thickness of the more strained part is $\sim$1000 nm and that of the less strained part of the film is $\sim$1200 nm thick, which is consistent with the AFM measurements. The XTEM also reveals that there is an abrupt interface between the two domains. In the more strained part of the layer a mottled contrast can be seen, which is interpreted as the presence of a high density of point defects, as reported in case of TiN.[28] This could explain the large component of isotropic strain in the more strained domains measured by XRD (see Table I). The less strained region is free from such a mottled contrast, indicating a lower density of point defects. Some threading dislocations that originate at the interface to the substrate can be seen inside the less strained regions.

Figure 9 shows a cross sectional HAADF STEM image from a larger region covering two less strained domains (A and C) and a more strained domain (B) in between them. The mottled contrast associated with point defects, previously observed in the more strained domain in the bright field image of Fig. 8, is recognized here in the whole B

Downloaded 13 Feb 2012 to 130.236.83.30. Redistribution subject to AIP license or copyright; see http://jap.aip.org/about/rights_and_permissions

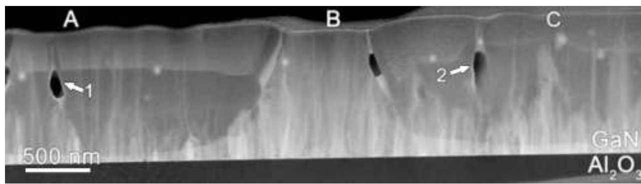

FIG. 9. Cross-sectional HAADF-STEM image from a thick sample with two less strained domains on the left and the right side of the image (A and C), and a more strained domain in between (B).

domain region and in the topmost ~200 nm of the less strained regions (A and C). Thus, region B has a higher density of point defects compared to the A and C regions. Additionally, as can be seen from Fig. 8, the threading dislocations are more abundant in region B compared to the less strained regions. The less strained regions (A and C) have a rounded bottom shape with the more strained region B extending in underneath the A and C regions from their sides to a minimum thickness of ~50 nm below their centers. This indicates that the more strained parts of the layer nucleated as film on the substrate before the less strained regions started to form. In comparison to the previously presented homogeneous GaN epilayers grown by DC-MSE, the more strained regions look rather similar, however, with a more mottled contrast in TEM and with a higher isotropic strain component detected by XRD.[9] In order to understand the formation of the strained domains, we note that in a high power impulse plasma process there is a high flux of energetic ions[29] along with reflected neutrals with a peak kinetic energy of a few hundred eV (the maximum applied potential in a pulse). This leads to the generation of point defects in the atomic layers of the GaN during the collision cascade from the energetic bombarding species.[30] This process is also known as atomic peening. This induces the observed mottled contrast in TEM and the isotropic strain component revealed by HRXRD.

Large voids 50-200 nm in size, two of them indicated by arrows 1 and 2, are clearly seen to have formed in the non-mottled parts of regions A and C and at the domain boundary. With STEM-EDX line scans it is possible to obtain the elemental distribution at a nanometer scale, i.e., very small amounts of elements can be detected at localized positions. The STEM-EDX line scans (not shown) revealed minute traces of Fe and Ni at the domain boundaries and inside the voids. However, the total amounts of these metal elements are smaller than the detection limits of ERDA, which average over a large area. The most probable source of these elements is the stainless steel crucible used to contain the liquid gallium. In the case of HiPIMS, the plasma is more evenly distributed over the target surface compared to the DC process and there is a possibility that the edges of the crucible may have been in contact with the plasma during the process, causing some sputtering of the stainless crucible. In the case of DC-MSE, the plasma is confined to the race track region above the liquid Ga surface and no such sputtering is possible. These elements, Fe and Ni, do not appear to be incorporated into the lattice and they seem to diffuse out to the boundaries of the less strained domains and into the voids. No mottled contrast is observed along those boundaries, indicating that the diffusion process of these metal trace elements may play a role in the elimination of the point defects.

The growth of less strained domains during film deposition is driven by the free energy reduction of the system, e.g., by out diffusion of point defects. Their nucleation may be triggered by a variety of reasons such as liquid Ga nano-droplets, Fe and Ni atoms arriving from the source, or the spontaneous formation of inversion domains. Once the nucleus is formed, the diffusion of point defects from the nucleus surroundings will lead to less strain due to the clustering of the point defects. The irregular shapes of the voids indicate a non-equilibrium state, which is consistent with an ongoing diffusion process, however slow due to the low growth temperature. Such a diffusion process could also lead to the observed elimination of threading dislocations from the less strained regions. It is, however, beyond the scope of this article to investigate this phenomenon in detail.

From the previous discussion, it is clear that high power pulses during the growth of GaN generate the point defects. Further work is required to find a stable process window involving less energetic ions to reduce the point defect density. This may be achieved, e.g., by applying a pulse retarding substrate potential to reduce the ion energies. Furthermore, enhancing the plasma density in the substrate vicinity would allow for a high flux of low energy ($<\sim$50 eV) ions which promotes a high adatom mobility. A better understanding of the diffusion process for metallic impurities in these domains may also help us to grow the relaxed GaN films directly on sapphire with good structural and optical properties.

In order to investigate the optical properties at room temperature and at low temperature (4 K), μ-PL was performed. Low temperature spectra from a less strained domain and a more strained domain in a GaN film grown at $P_{N2} = 9$ mTorr are shown in Fig. 10(a). The spectrum from the less strained GaN exhibits strong band edge luminescence at 3.47 eV with a FWHM of 10 meV. The high intensity and narrowband edge luminescence peak confirm the high structural quality of the less strained GaN domains determined by XRD, μ-Raman, and TEM. The position of the band edge peak also indicates that the material is almost fully relaxed. The spectrum from the more strained part shows a band edge luminescence at 3.48 eV with a broader FWHM of ~14 meV. The shift in the peak position indicates a compressive strain in the film,[23] which is in agreement with the XRD and μ-Raman results. The lower intensity and broader peak corresponds to a lower structural quality of the more strained GaN compared to the less strained domains. Yellow luminescence, which is often observed in GaN films, is not observed in any of these spectra. Figure 10(b) shows the room temperature μ-PL spectra from the less strained and the more strained domains. Both spectra exhibit band edge luminescence at 3.43 eV with a FWHM of 58 meV for the less strained domains and a FWHM of 52 meV for the more strained domains. Thus, the peaks are red-shifted and broadened at room temperature, which is due to the lattice expansion and the carrier thermalization effects. At room temperature, one can also see yellow luminescence in both

Downloaded 13 Feb 2012 to 130.236.83.30. Redistribution subject to AIP license or copyright; see http://jap.aip.org/about/rights_and_permissions

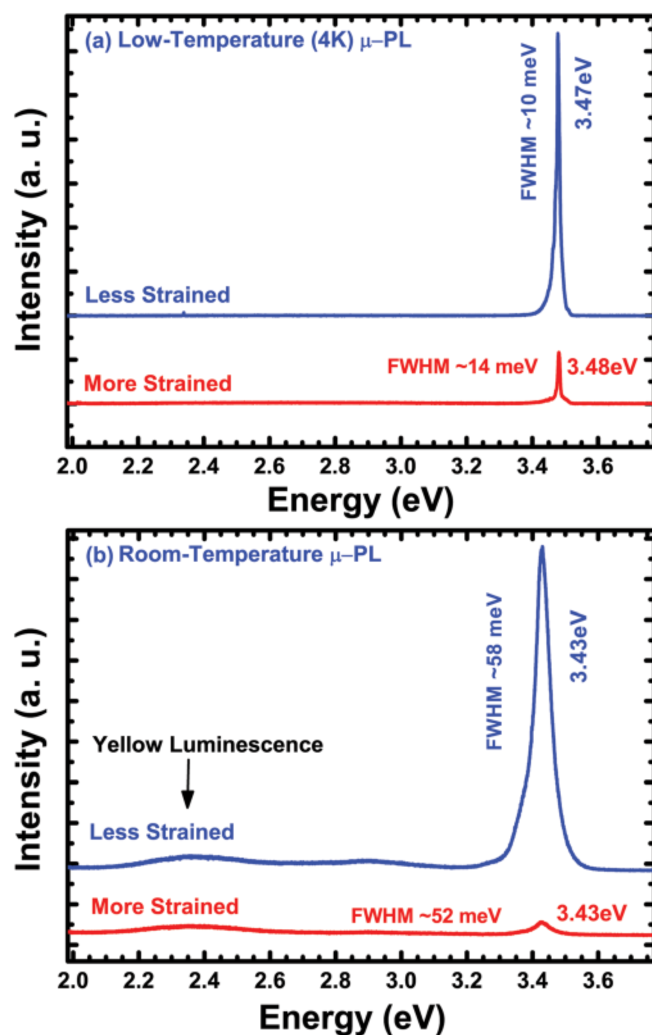

FIG. 10. (Color online) (a) Low temperature (4 K) μ-PL spectra from the less strained and the more strained domains. (b) Room temperature μ-PL spectra from the less strained and more strained domains.

spectra that is also common for MBE and CVD grown GaN.[31] The intensity ratios between the band edge luminescence and the yellow luminescence for the less strained and the more strained domains are 14.5 and 1.2, respectively. The room temperature luminescence indicates a semiconductor material of high quality with thermally activated defects, and it also confirms that the less strained domains have superior optical properties over the more strained parts.

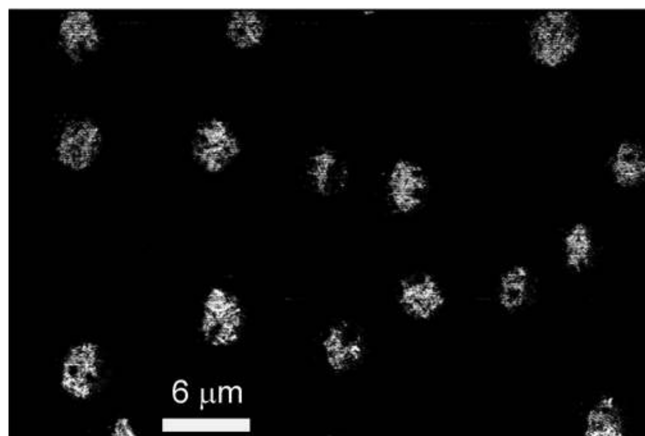

FIG. 11. (a) Room temperature panchromatic CL image showing the luminescence at room temperature from the less strained domains.

To see the spatial distribution of the less strained domains at room temperature, a panchromatic CL image was recorded and is shown in Fig. 11. It shows that the less strained features give rise to nearly all of the intensity, confirming a higher structural quality with less defects in those domains, which is in agreement with the room temperature μ-PL results.

IV. CONCLUSIONS

The GaN (0001) epitaxial layers can be grown directly onto Al_2O_3 substrates by a reactive MSE process using HiPIMS. Micrometer thick films, however, consist predominantly of compressively-strained domains that surround disk-shaped, almost fully relaxed, domains. The more strained domains are likely the result of highly energetic ion bombardment as a consequence of high power pulses used during deposition, causing a high point defect density, while the less strained domains form due to relaxation through a point defect diffusion process during growth. The two domain types have good structural and optical properties which are reflected in the XRD, μ-Raman, μ-PL, and CL data. More strained domains have an XRD ω-FWHM value of 1024 arc sec and a low temperature band edge luminescence peak at 3.48 eV, and the less strained domains have a corresponding ω-FWHM 885 arc sec and luminescence at 3.47 eV along with the expected Raman peak shift at 569.9 cm^{-1}. Additionally, room temperature luminescence from the relaxed domains is demonstrated by μ-PL and CL imaging. This study shows that high power impulse magnetron sputter epitaxy has the potential to grow high quality relaxed epitaxial GaN films directly on sapphire, provided that the mechanisms for the creation and diffusion of the point defects can be understood and controlled.

ACKNOWLEDGMENTS

This work was supported by the Swedish Foundation for Strategic Research through the MS^2E and Nano-N programs.

[1]S. C. Jain, M. Willander, J. Naryan, and R. Van Overstraeten, J. Appl. Phys. **87**, 3 (2000).
[2]M. S. Shur and R. F. Davis, *GaN-Based Materials and Devices* (World Scientific, Singapore, 2004).
[3]R. Quay, *Gallium Nitride Electronics* (Springer-Verlag, Berlin, 2008).
[4]S. Nakamura, Science **281**, 956 (1998).
[5]P. Waltereit, O. Brandt, A. Trampert, H. T. Grahn, J. Menniger, M. Ramsteiner, M. Reiche, and K. H. Ploog, Nature (London) **406**, 865 (2000).
[6]J. Wu, J. Appl. Phys. **106**, 011101 (2009).
[7]D. Ehrentraut and Z. Sitar, MRS Bull. **34**, 259 (2009).
[8]O. Ambacher, J. Phys. D: Appl. Phys. **31**, 2653 (1998).
[9]M. Junaid, C.-L. Hsiao, J. Palisaitis, J. Jensen, P. O. Å. Persson, L. Hultman, and J. Birch, Appl. Phys. Lett. **98**, 141915 (2011).
[10]J. Bohlmark, M. Lattemann, J. T. Gudmundsson, P. A. Ehiasarian, Y. Aranda Gonzalvo, N. Brenning, and U. Helmersson, Thin Solid Films **515**, 1522 (2006).
[11]M. Samuelsson, D. Lundin, J. Jensen, M. A. Raadu, J. T. Gudmundsson, and U. Helmersson, Surf. Coat. Technol. **205**, 591 (2010).

Downloaded 13 Feb 2012 to 130.236.83.30. Redistribution subject to AIP license or copyright; see http://jap.aip.org/about/rights_and_permissions

[12]V. Kouznetsov, K. Macák, J. M. Schneider, U. Helmersson, and I. Petrov, Surf. Coat. Technol. **122** 290 (1999).
[13]E. Wallin and U. Helmersson, Thin Solid Films **516**, 6398 (2008).
[14]J. Whitlow, G. Possnert, and C. S. Petersson, Nucl. Instrum. Methods Phys. Res. B **27**, 448 (1987).
[15]M. S. Janson, CONTES, Conversion of Time-Energy Spectra, a program for ERDA data analysis. Internal Report, Uppsala University, 2004).
[16]C.-L. Hsiao, L.-W. Tu, T.-W. Chi, M. Chen, T.-F. Young, C.-T. Chia, and Y.-M. Chang, Appl. Phys. Lett. **90**, 043102 (2007).
[17]S. Dhara, C. R. Das, H. C. Hsu, B. Raj, A. K. Bhaduri, L. C. Chen, K. H. Chen, S. K. Albert, and A. Ray, Appl. Phys. Lett. **92**, 143114 (2008).
[18]T. Seppänen, L. Hultman, and J. Birch, Appl. Phys. Lett. **89**, 181928 (2006).
[19]T. Metzger, R. Hopler, E. Born, O. Ambacher, M. Stutzmann, R. Stommer, M. Schuster, H. Gobel, S. Christiansen, M. Albrecht, and H. P. Stunk, Philos. Mag. A **77**, 1013 (1998).
[20]V. Darakchieva, B. Monemar, and A. Usui, Appl. Phys. Lett. **91**, 031911 (2007).
[21]J. M. Wagner and F. Bechstedt, Phys. Rev. B **66**, 115202 (2002).
[22]M. Yamaguchi, T. Yagi, T. Azuhata, T. Sota, K. Suzuki, S. Chichibu, and S. Nakamura, J. Phys.: Condens. Matter **9**, 241 (1997).
[23]C. Kisielowski, J. Krüger, S. Ruvimov, T. Suski, J. W. Ager III, E. Jones, Z. Liliental-Weber, M. Rubin, and E. R. Weber, Phys. Rev. B **54**, 17745 (1996).
[24]C. G. Van de Walle, Phys. Rev. B **68**, 165209 (2003).
[25]V. Yu. Davydov, Yu. E. Kitaev, I. N. Goncharuk, A. N. Smirnov, J. Graul, O. Semchinova, D. Uffmann, M. B. Smirnov, A. P. Mirgorodsky, and R. A. Evarestov, Phys. Rev. B **58**, 12899 (1998).
[26]L. Bergman, D. Alexson, P. L. Murphy, R. J. Nemanich, M. Dutta, M. A. Stroscio, C. Balkas, H. Shin, and R. F. Davis, Phys. Rev. B **59**, 12977 (1999).
[27]V. Darakchieva, T. Paskova, M. Schubert, H. Arwin, P. P. Paskov, B. Monemar, D. Hommel, J. Off, F. Scholz, M. Heuken, B. A. Haskell, P. T. Fini, S. J. Speck, and S. Nakamura, Phys. Rev. B **75**, 195217 (2007).
[28]I. Petrov, L. Hultman, U. Helmersson, J.-E. Sundgren, and J. E. Greene, Thin Solid Films **169**, 299 (1989).
[29]D. Lundin, P. Larsson, E. Wallin, M. Lattemann, N. Brenning, and U. Helmersson, Plasma Sources Sci. Technol. **17**, 035021 (2008).
[30]M. Ohring, *Materials Science of Thin Films: Deposition and Structure*, 2nd ed. (Academic, San Diego, CA, 2002).
[31]A. Reshchikov and H. Morkoc, J. Appl. Phys. **97**, 061301 (2005).

Downloaded 13 Feb 2012 to 130.236.83.30. Redistribution subject to AIP license or copyright; see http://jap.aip.org/about/rights_and_permissions